Chemical Engineering Journal 289 (2016) 203–211

Contents lists available at ScienceDirect

Chemical Engineering Journal

journal homepage: www.elsevier.com/locate/cej

Free surface electrospinning of aqueous polymer solutions from a wire electrode

Indrani Bhattacharyya, Mark C. Molaro, Richard D. Braatz, Gregory C. Rutledge *

Department of Chemical Engineering and Novartis-MIT Center for Continuous Manufacturing, Massachusetts Institute of Technology, Cambridge, MA 02139, USA

HIGHLIGHTS

- Fibers are formed from aqueous solution by free surface electrospinning from a wire.
- Productivity entails liquid entrainment, film breakup, and electrified jetting.
- Changes of equipment design, operation and modeling are presented.
- A productivity model for manufacturing of fibers by this process is validated.

ARTICLE INFO

Article history:
Received 23 June 2015
Received in revised form 11 December 2015
Accepted 14 December 2015
Available online 24 December 2015

Keywords:
Electrospinning
Nanofiber
Poly(vinyl alcohol)
Productivity
Needleless electrospinning

ABSTRACT

The production of nanofibers from an aqueous solution of poly(vinyl alcohol) by the method of free surface electrospinning from a wire electrode has been examined. The results are interpreted in terms of a previously reported model that was based on the production of fibers from polymeric solutions in ethanol by the same method. Differences in behavior were observed between the processing of aqueous and ethanolic solutions, arising from the more viscoelastic nature of the aqueous solution, the higher surface tension, the fewer number of droplets jetting simultaneously from the wire, and the different electrical current profile observed for jetting from a single droplet. These differences necessitated changes in equipment design, operation of the process, and modeling of productivity. The result is a more robust model for the productivity of fibers by free surface electrospinning from a wire electrode.

1. Introduction

With the ever-increasing popularity of nanotechnology, electrospun fibrous materials have drawn attention for their potential applications in such areas as energy storage, drug delivery, tissue engineering, filtration, and defense and security [1,2]. The main advantage of electrospinning technology over other fiber-forming techniques is its ability to generate non-woven mats with fibers less than 1 mm in diameter and with high surface-to-volume ratio. Traditionally, the electrospinning technique uses an electrically charged metal needle or spinneret to feed a viscoelastic liquid into a continuously operating, electrically-charged jet. A grounded metal plate at a certain distance from the needle tip is used as a collector for the fibers, which usually dry before they reach the collector due to the high surface area of the jet made possible by the electrical stretching forces. However, a major drawback of traditional electrospinning with a single needle spinneret is low throughput, usually 0.1–1 g/hr/needle, depending on solution and process parameters [3], which has limited the use of the traditional technique in industrial settings. Several different ways of increasing the throughput of electrospun fibers have been studied over the past few years, from the use of arrays of single-needle spinnerets to a wide variety of other configurations that may collectively be called "needle-less" or "free surface" electrospinning methods [3–6].

Free surface electrospinning is a technique that takes advantage of the remarkable capacity to launch multiple jets from a charged liquid surface, in principle, if the surface charge density is high enough and curvature can be introduced to the air–liquid interface [7]. One of the earliest configurations of free surface electrospinning employed a magnetic liquid to create liquid "spikes" that perturbed the charged liquid surface. Since then, numerous configurations have been reported to induce free surface electrospinning, e.g., liquid-filled trenches, slits, wetted spheres, rotating wires and fixed wires, cylinders, disks, conical wire coils, and gas bubbles rising through the liquid surface [3,6,8–15]. Many of these approaches have shown promising increase in throughput, and a number of reviews are available [16–18]. However, for implementation of a process in an industrial setting, a thorough and

* Corresponding author.

http://dx.doi.org/10.1016/j.cej.2015.12.067
1385-8947/

quantitative understanding of the design parameters is required. Choosing a relatively simple design for high throughput electrospinning allows one to analyze the process for important factors that affect the throughput and product quality.

In a previous paper [9], free surface electrospinning from a wire electrode was analyzed to understand the effects of different process parameters and solution properties on productivity of fiber, and an empirical model was developed using solutions of poly (vinyl pyrrolidone) (PVP) in ethanol as the fluid. In that work, a relatively simple experimental design was used, in which a wire electrode was connected to high voltage power supply and mounted on a rotating spindle such that the electrode both charged the fluid and delivered it into the high electric field [9]. Details of the equipment design were described there [9]. The entire electrospinning process was decomposed into a sequence of three steps: (i) the entrainment of liquid on the wire as it passes through a liquid–air interface, (ii) the breakup of an annular layer of liquid into droplets on the cylindrical wire, and (iii) the formation of jets from the droplets by electrostatic forces. A review of the understanding of each of these steps was provided previously by Forward and Rutledge [9]. Briefly, the amount of liquid entrained on the wire was found to be predominantly a function of the capillary number, $Ca = u\eta/\gamma$, where u is the velocity of the wire, η is the fluid viscosity and γ is the fluid surface tension. Once entrained, the cylindrical layer of liquid on the wire would break up into droplets by a Plateau–Rayleigh instability. The separation distance between droplets is dominated by the most rapidly growing disturbance, whose wavelength λ is a function of the radius a_0 of the annular liquid surface and the Ohnesorge number, $Oh = \eta/(\rho\gamma r)^{1/2}$, where ρ is the density of the liquid and r is the radius of the wire [19]. For low levels of entrainment, ($a_0/r < 2$) the wavelength should be approximately constant ($2\pi a_0/\lambda \sim 0.69$), but Forward and Rutledge [9] found it to depend on applied voltage as well. Once formed, the droplets on the charged wire emit jets above a critical threshold of the local electric field. Since the wire was mounted on a rotating spindle, the local electric field at the wire was a function of angular position, with a maximum at the apex of rotation. It was also observed that the droplets did not all jet simultaneously. This observation was explained to be a consequence of the electrostatic fields created by nearby jets, which suppress simultaneous jetting from neighboring droplets. The linear jet density distribution was characterized by measurements of the electrical current flow at the collector for single jets and for multiple jetting of droplets on the wire, and reported to be a function of local electric field at the wire. These observations were used to construct a model of productivity for the PVP/ethanol system as a function of solution properties (i.e. surface tension, viscosity, density and concentration) and process parameters (rotation rate and electric field). Details of this model are described elsewhere [9].

In this report, we extend the applicability of this productivity model to aqueous solutions of poly(vinyl alcohol) or PVA. The applicability of this model to aqueous solution systems is not obvious because of the significant differences in solution properties and viscoelastic behavior of aqueous PVA solutions from ethanolic PVP solution. A comparison of solution properties between PVP/ethanol and PVA/water is given in Table 1. As we apply the model to aqueous polymeric solution, we also report some new observations and accommodate them in the model as required.

Table 1
Comparison of solution properties of 7 wt% PVA/water (this work) and 30 wt% PVP/ethanol (Ref. [9]).

Material	146–186 kDa PVA	55 kDa PVP
Concentration (wt%)	7	30
Density, ρ (kg/m^3)	1075	0.898
Conductivity (S/m)	0.0633	8.89×10^{-4}
Viscosity, η (Pa s)	0.520	0.105
Surface tension γ (N/m)	0.0495	0.023
Ohnesorge number, Oh	7.22	2.3

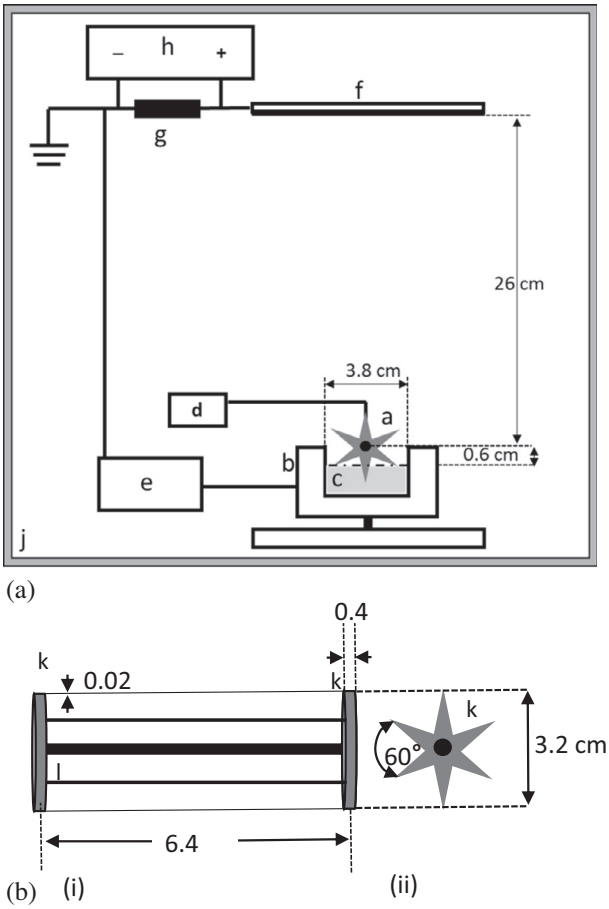

Fig. 1. (a) Schematic of the apparatus for free surface electrospinning from wire electrodes on a star-shaped spindle. The components are: (a) wire electrode, (b) solution bath, (c) solution, (d) DC motor, (e) high voltage power supply, (f) collector plate, (g) 1 MΩ resistor, (h) multimeter, (j) enclosure box. Refer to text for description of the apparatus. (b) Schematic of the wire electrode with spoked wheels (k) and threaded rod (l); (i) side view, perpendicular to spindle axis, (ii) end-on view, parallel to spindle axis. All dimensions are in cm.

2. Experimental method

2.1. Experimental apparatus

The apparatus is shown in Fig. 1a; it consisted of several different components as described below. A wire electrode spindle (a) was placed in a bath (b) filled with polymer solution (c). The spindle was rotated by a DC motor (Zheng gear box motor ZGA25RP216) that was driven by a power supply (d). The rotation speeds ranged from 1.6 to 8.7 rpm; this corresponds to wire velocities u of 0.5–2.7 cm/s. The shear rate $\dot{\gamma} = u/z$ at the wire was ~100–700 s^{-1}, where $z = a_0 - r$ is the thickness of the liquid coating on the wire. The liquid in the bath was electrified by a high voltage power supply (e) that was connected to the metal pin at the bottom of the bath. A metal plate (f) collected the non-woven fibers. The metal plate was connected to a 1 MΩ resistor (g) across which the voltage drop was measured by a multi-meter (h) in order to quantify the current flow to the collector plate. The whole set-up

was placed in a Plexiglas® chamber (j) inside which the relative humidity was maintained at 20% by a humidity controller (ETS, Model: 5100) for most of the experiments.

In order to electrospin a solution using a wire electrode successfully, the events of liquid entrainment, break-up of droplets and jetting should occur promptly and sequentially. However, due to the highly viscoelastic nature of the aqueous solutions of PVA used in this work, a stable film of liquid frequently formed between the consecutive wires on the spindle. Hence, a cylindrical layer of liquid could not form around the wire within the time that the electrode resided in the regime of electric field in excess of the critical value. In order to promote consistent annular liquid entrainment and thereby facilitate the following droplet break-up, the spindle was modified as follows to prevent film formation and allow successful electrospinning of aqueous PVA solutions. The round Teflon wheels of Ref. [9] were replaced by two spoked wheels (k) made of Ultem® to hold the wires in place. The wheels were held in place on a threaded rod (l) by nuts. Grooves centered on the end of each spoke held the stainless steel wires in place. A wire of diameter 200 μm was strung between spokes on the two wheels, as shown in Fig. 1b, to create the spindle. Up to six wires could be accommodated on the spindle. However, in this work, only two wires were used, 180° apart from each other.

2.2. Solution preparation

Poly(vinyl alcohol) (PVA) with Mw = 146–186 kDa (87% hydrolyzed) was obtained from Sigma–Aldrich. A 7 wt% polymer solution in de-ionized (DI, laboratory supply) water was used in these experiments. Viscosities were determined using an AGR2 Rheometer (TA Instruments). The liquids showed Newtonian behavior for shear rates below 1000 s^{-1}. Conductivities were measured with a VWR Traceable digital conductivity meter. Surface tensions were measured using a Krüss K100MK2 Processor–Tensiometer. Solution properties are listed in Table 1. It is important to notice here that the aqueous PVA solution is not only five times more viscous than PVP/Ethanol solution, but also has a significantly higher surface tension and electrical conductivity as well.

2.3. Measurement of entrained liquid layer

In order to determine the total volume of solution entrained on a wire, the droplets formed on the wire after de-wetting of the entrained liquid were imaged, and their volumes were determined using Carroll's equations for barrel-shaped drops [20]. The total volume of the liquid was then determined by summing the liquid droplet volumes. Images of the droplets on the wire were recorded photographically with a 1st Vision MC 433 Firewire Camera and Quantaray AF 70–300 mm f/4.0–5.6 LD Tele Micro Lens. Image J software (National Institute of Health) was used to measure the equatorial height, length, contact angle between the liquid layer and the wire, and the center-to-center distance (λ) between the droplets. The contact angle was found to be relatively constant, with a value of 5° ± 3°. The diameter of the wire was kept constant (200 μm) throughout all the experiments. Satellite droplets were observed in between the major droplets, as shown in Fig. 2. Their volumes were obtained by the same method and added to the volumes of major droplets in order to obtain the total volume of entrained liquid. A MATLAB routine was used to calculate the shape and volume (V_d) of a droplet, to a tolerance of 0.01% [9]. For detailed description of the algorithm for determining V_d, the reader is referred to [9] To obtain an average value for volume and center-to-center-distance, measurements were taken over at least 100 droplets. Using the volumes of the droplets and the number of droplets on a wire, an equivalent thickness (z) of the entrained annular liquid layer on a wire was calculated, using the equation:

$$z = \left(\frac{V_d}{\pi\lambda} + r^2\right)^{1/2} - r \quad (1)$$

2.4. Electrospinning and current measurements

In order to initiate electrospinning, a high potential was applied to the solution bath. The wire electrodes were also connected to the same applied voltage, to ensure that the surface of the bath and the wires were at the same potential as the external power supply. The applied potential was increased slowly until at least a few of the droplets on the wire formed Taylor-like cones and finally emitted jets. The droplets on a wire did not all jet simultaneously. The number of droplets jetting at any given time varied depending on the applied potential. The volume of each droplet varied during the lifetime of its jet, as liquid was removed by the jet itself. Also, the local electric field around a droplet varied due to motion of the wire through the arc of rotation.

As the jets travelled through the chamber, water evaporated and dry solid PVA fibers were deposited on a copper plate collector at a distance of 26 cm from the central rod of the electrode spindle. In order to monitor the electrical charge carried by the liquid to the collector in the form of jets, the voltage drop was measured across a 1 MΩ resistor between the collector and true ground (Fig. 1a). This current flow was assumed to be that due to free charge remaining on the fibers at time of deposition; it is possible that some charges were carried away by the evaporated solvent [21]. The relative humidity within the chamber was maintained at 20%. It was observed that if the relative humidity was higher than 20%, the critical field required to initiate jetting increased; this effect was attributed to dissipation of surface charge at the droplets by excessive moisture. The potentials applied in these experiments were below 55 kV, which is significantly lower than the threshold of 126 kV/cm required for corona discharge in air at standard temperature and pressure. A measurement of the background current, performed without any solution in the bath and under the application of the same potential as was used during the spinning experiment, confirmed that corona discharge was not significant.

To avoid any changes in solution properties over the duration of electrospinning due to evaporation of solvent from the bath itself, the experiments were limited to a maximum duration of 15 min. In

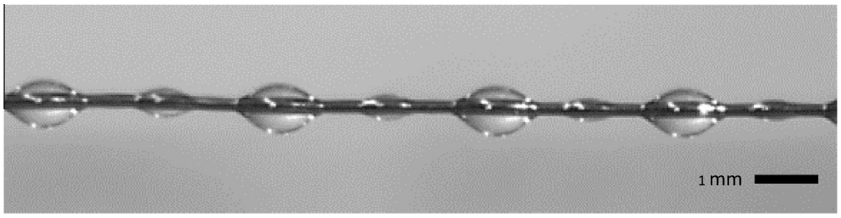

Fig. 2. Formation of satellite droplets of aqueous solution of PVA (7 wt%) on the wire, midway between mother droplets.

any case, "solution aging" was much less prominent for aqueous solutions of PVA, than for the ethanolic solutions of PVP used in Ref. [9]. The masses of the deposited electrospun mats were measured after each experiment using a micro-balance.

2.5. Electric current analysis

Under the conditions for these experiments, the measurement of a finite electric current (or voltage) across the 1 MΩ resistor was considered to be a reliable indication of jetting behavior. In order to estimate the total volumetric flow of liquid in the form of jets, the total current was measured continuously throughout the arc of rotation of the wire electrode. In order to deconvolute subsequently the total electric current into contributions from several individual jets, the current from a single jet was measured as well. Multiple experiments were conducted in which the effective length of the wire was reduced by covering the wire with insulating tape, leaving a small portion exposed such that only three to four droplets could form after the wire was coated with liquid at each rotational speed and applied potential. Of those three to four droplets, only one droplet could jet within one rotation of the wire. By analyzing the data for electric current versus time, for both a wire supporting multiple jets and one supporting a single jet, a quantitative measure of the jet density along the wire could be obtained.

In this work, a statistical model was developed to deconvolute the measured current signal into contributions from individual droplets. In their previous work, Forward and Rutledge used a deconvolution strategy based on the assumption that each individual jet produced the same current profile, and that these may be combined additively to produce the overall measured current [9]. This assumption of the same current profile for each jet was found not to hold for the solutions studied in this work. Thus, a new approach was taken to analyze the present data. The model used to fit the data in this work made several simplifying assumptions. Firstly, the single jet current profile was approximated as piecewise linear. The data was modeled assuming independent and identically distributed Gaussian noise. The model allowed for multiple jets to occur simultaneously, or with overlapping periods of contact with the collection plate. Jet currents were assumed to be additive. The time domain was discretized in accordance with the sampling rate of the electrical signal. For more details of the model used to describe multiple jetting and its solution as an optimization problem, the reader is referred to the Supporting Information.

2.6. Estimating the electric field around the wire electrode

A 2D finite element method (FEM) electrostatics model implemented in COMSOL Multiphysics® 4.0 Modeling Software was used to calculate static electric field around the wire electrode placed between two charged finite-sized planes (the solution bath with applied potential and the grounded collector plate). The simulation did not take into account the liquid entrainment, the droplets and the presence of liquid jets from the droplets. The electrostatic equations were solved over a rectangular geometry consisting of the air between solution bath (dash–dot line showing the upper level of solution (c) in Fig. 1(a)) and collector plate (bold line showing the lower surface of the metal plate (f)) and the electrode wire. The electric field at the surface of a 200 μm wire was modeled under the application of 45 kV potential. The model was meshed and solved for the electric field at the wire at 19 angular positions along the arc of rotation of the wire about the spindle axis. At each wire location, the model was solved using zero charge boundary conditions on the sides of the domain, the collector plate set as ground potential, and the solution bath and wire held at the applied potential of 45 kV. The results for electric field at the wire are well-described by a second degree polynomial in φ, the angular position of the wire electrode:

$$\frac{E_w(\varphi)}{V_{\text{appl}}} = A_1\varphi^2 + A_2\varphi + A_3 \tag{2}$$

with A_1, A_2, and A_3 equal to -4.5×10^{-5} deg^{-2} cm^{-1}, 0.0083 deg^{-1} cm^{-1}, and 0.685 cm^{-1}, respectively; these values are dependent upon the geometry of the apparatus.

3. Results and discussion

3.1. Liquid entrainment

The entrainment of liquid on the wire was examined for aqueous PVA solution. With dilute solutions of PVA in water, only barrel-shaped droplets were observed, as was the case with PVP/ethanol solutions [9]. The formation of small satellite droplets in between the larger "mother" droplets was observed in the case of these aqueous PVA solutions. However, the volume of the satellite droplets was only 3% of the total volume of the mother droplets. The satellite droplets were barrel-shaped as well (Fig. 2).

The normalized film thickness is expected to scale with capillary number Ca according to a power law relation, as observed previously by Goucher, Quéré, and Forward [9,22,23]:

$$\frac{z}{r} = a(Ca)^b \tag{3}$$

For $Ca < 0.20$, the normalized film thickness was well-described by $a = 2.06 \pm 0.08$ and $b = 0.21 \pm 0.02$ with an $R^2 = 0.95$ (see Fig. 3). The film thickness appeared to reach a plateau as the capillary number increased beyond 0.20. The relationship of normalized film thickness to capillary number beyond 0.20 was found to be approximately linear with a slope of 0.21. Beyond $Ca \sim 0.40$, the desired annular liquid film was observed not to form on the wires, due to the relatively high spindle rotation rate compared to the time required for breakup of the film that formed between the wires, and the short residence time of the wire within the electric field for jet initiation. Thus, due to the highly viscoelastic nature of the PVA solution, there exists an upper limit in rotation rate beyond which jetting, and fiber formation, was not observed. Nevertheless, for a given rotation rate, the entrainment of liquid on the wire was observed to be much higher for the aqueous PVA solutions studied here, compared to the solutions of PVP in ethanol reported previously [9]. This increased entrainment can be attributed to the higher viscosity of the aqueous PVA solution, resulting in slower drainage of liquid back to the bath.

3.2. Influence of electric field on the wavelength parameter

The wavelength parameter serves as a measure of the distance between the droplets in relation to the thickness of the annular liquid layer on the wire. With increase in rotation rate of the spindle, the amount of liquid entrained increased. The center-to-center distance between the droplets was observed to change systematically with rotation rate. In the absence of any applied potential, the average value of wavelength parameter was found to be 0.44 ± 0.02.

In contrast to ethanolic solutions of PVP, the PVA/water system exhibited almost no effect of applied potential on λ, according to the relationship between $2\pi a_0$ and λ given by

$$\frac{2\pi a_0}{\lambda} = 0.0013V_{\text{Appl}} + 0.44, \tag{4}$$

where V_{Appl} is given in units of kV (see Fig. 4). This relationship is attributed to the dominance of viscoelastic forces of the liquid over electrostatic forces on the droplet breakup.

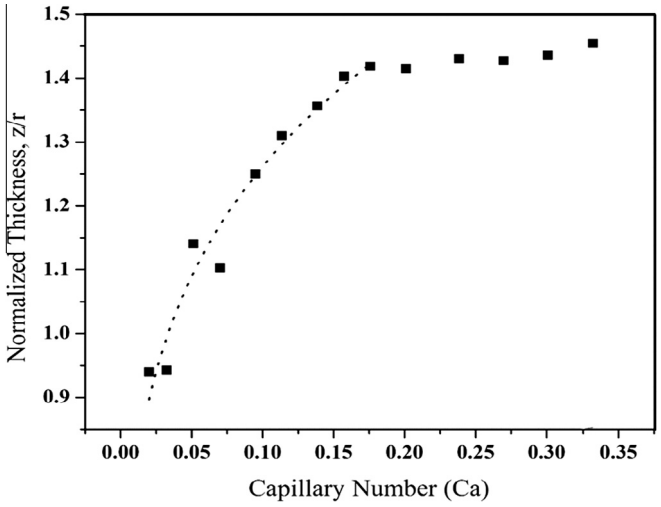

Fig. 3. Liquid entrainment of 7 wt% aqueous PVA (146–186 kDa) solution. Black dotted line is the power law fit to the data.

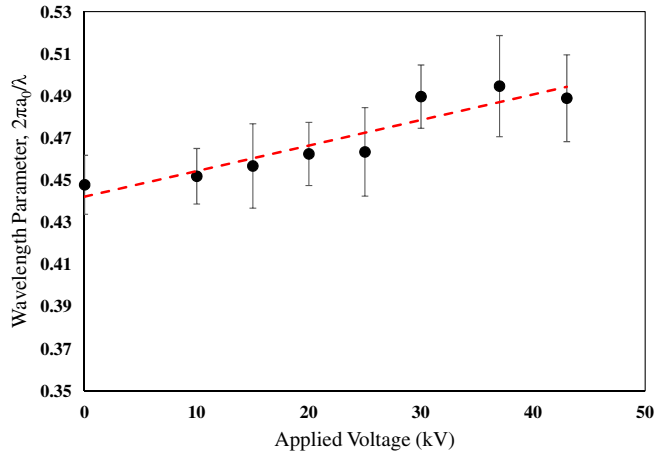

Fig. 4. The correlation between wavelength parameter, $2\pi a_0/\lambda$, and applied electric potential at a constant spindle rotation rate of 2.5 rpm.

3.3. Jet initiation and termination

As the spindle rotates and the electrode wires travel up through the liquid–air interface, the distance between the wire and the grounded collector plate continuously changes. Thus, the electric field strength on the wire changes along the arc of rotation. With increasing voltage applied to the solution bath and the wires, the droplets on the wires were observed to deform from the symmetric barrel-shaped droplets, exhibiting an increasingly prominent conical shape, culminating in emission of a jet. As was the case observed previously for PVP/ethanol solutions, jetting was found to occur when conditions at the wire exceeded a critical field strength. From observations of the height of the wire above the surface of the solution bath at the moment of initiation of the first jet (refer to Fig 1 for geometry, with the reference angle of 90° corresponding to the apex of rotation), the angular position of the wire was determined, and the electric field on the wire at that position was obtained from Eq. (2). For five different applied potentials in the range of 37–50 kV, the critical field strength for jet initiation was found to occur at 38 ± 2.1 kV/cm, about 10% higher than the critical electric field observed for PVP/ethanol systems (34 ± 1.3 kV/cm). This difference is attributed to the higher viscosity and surface tension of the aqueous PVA solutions. The implication of the critical electric field condition for jetting is that a larger applied potential on the wire results in a larger angular range where jetting is possible, while a faster rotation speed reduces the time spent by the wire within this angular range. However, in contrast to the PVP/ethanol solutions, aqueous PVA solutions were observed to continue jetting even after the wire exited the angular range in which the critical field strength was exceeded, as confirmed by electric current measurements. This indicates that there exists some hysteresis in the electric field dependence of jet initiation and termination. Such hysteresis was also reported by Shin et al. [24] for a needle-based apparatus. Fig. 5(a) presents some typical results for electric current measured as a function of angular position of the wire. It is immediately apparent that jetting generally initiates at the same point (~23.5° for V_{Appl} = 45 kV), but is generally not symmetric about the apex of the arc of rotation (90°). The angular range of jetting versus rotation rate of the spindle is plotted in Fig. 5(b). It can be seen that the angular range of

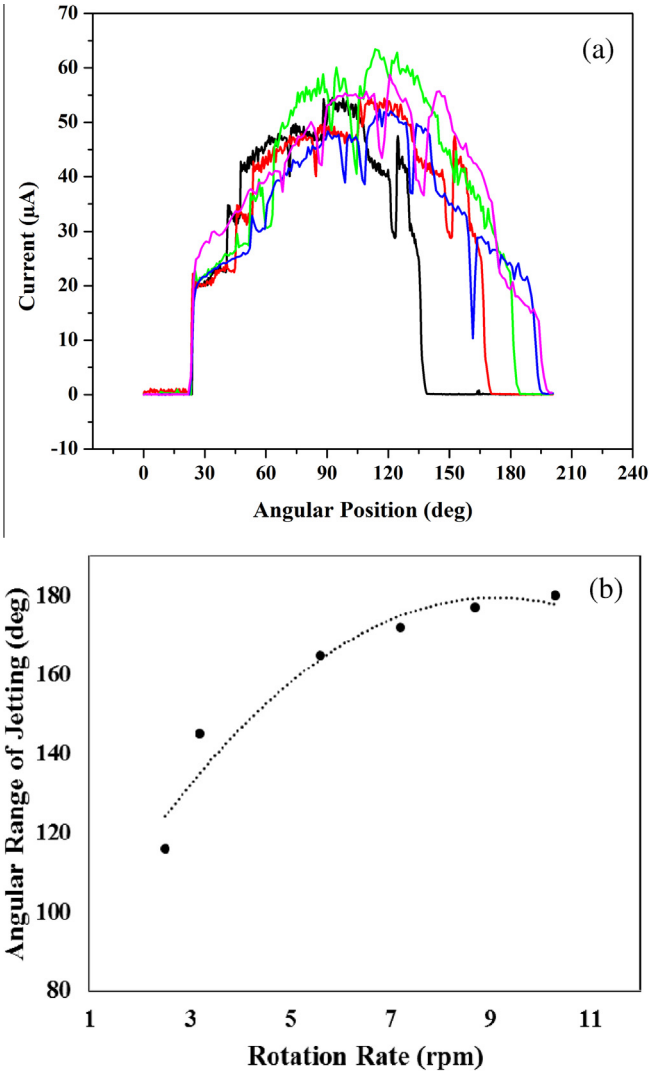

Fig. 5. (a) Current drawn from 7 wt% PVA/water solution at 45 kV under different spindle rotation rates of 2.5 rpm (black), 3.2 rpm (red), 5.6 rpm (green), 7.2 rpm (blue) and 8.7 rpm (magenta) as a function of angular wire position. The differences in electric current profiles are indicatively of the variation in jetting with spindle rotation rate. (b) Angular range of jetting vs. rotation rate of spindle for an applied voltage of 45 kV. The dotted line is a guide to the eye.

jetting from initiation to termination increases slowly with rotation rate and apparently plateaus at high rotation rate. For rotation rates below 5 rpm, the entrained liquid on the wire electrode is completely depleted by jetting before the wire travels the full angular range (i.e., 23.5°–156.5°) in which the electric field is above the critical value of ~38 kV; this behavior has been called the "entrainment-limited regime" [9]. For rotation rates above 5 rpm, jetting continues throughout the angular range in which the electric field is above critical, and even beyond this, to angles as large are 203°. Under these conditions, jetting is limited not by the amount of liquid entrained on the wire, but by the amount of liquid that can be jetted from the wire electrode in the time required for the electrode to travel from the position at which the electric field is sufficient to initiate jetting, to the position at which the electric field falls below the value required to sustain jetting. Thus, this behavior has been called the "field-limited regime".

3.4. Single jet lifetime

The current measurements such as the one shown in Fig. 5(a) are constituted of contributions from many individual jets. In order to estimate the total volume of liquid jetted from each wire in the field-limited regime, it was necessary to deconvolute the wire current into a summation of several individual jet currents. For this purpose, the current originating from a single jet was measured at different rotation rates. An average over at least 10 jets was taken for an applied voltage of 45 kV, and the single jet current versus time is plotted in Fig. 6. The average lifetime of a single jet of PVA/water solution was calculated to be t_J = 1.6 s and was considered to be independent of applied voltage for the purposes of predicting productivity.

In another set of experiments, drops on the wire were allowed to jet only after the wire crossed its apex of rotation (by keeping the voltage off until the wire reached the apex). It is interesting to note that the current profiles for individual jets initiating at different angular positions were not similar. In the first half of rotation, i.e., before reaching the apex of the arc of rotation, the current profile was observed to have an increasing slope in the middle, as shown in Fig. 6. However, if a droplet was allowed to jet in the second half of the rotation, i.e., after reaching the apex of rotation, the current profile had a decreasing slope in the middle. These observations contrast with those of Ref. [9].

3.5. Jet lifetime and frequency

The contribution of individual jetting droplets to the total measured current versus time was estimated by fitting a Bayesian model to the data. As described in the Supporting Information, a simplified model for a single jet profile introduces $5n_{jets}$ parameters to be estimated by fitting to the measured current versus time profile for a wire having many jetting droplets. In general, this problem may be underdetermined. This modeling method requires the determination of a large number of parameters from a limited amount of available data. To improve the tractability of the analysis, the solution space was narrowed by inclusion of constraints on the allowable ranges of parameters, and by the introduction of penalty terms in the final fitting procedure to include the prior knowledge for expected values of these parameters in the physical scenario being mathematically modeled.

For a given set of experimental conditions, the measured volume of a droplet was observed to vary less than 3%. Similarly, the total charge associated with a droplet, as determined by integration of the current versus time profiles, was observed to vary with coefficient of variation < 0.1. From 40 to 60 single jet measurements at each experimental condition, the integral of the current versus time was calculated. These experimental observations were used to introduce a Bayesian component to the data model. The prior distribution included was a normal distribution for the total charge transferred by a jet, with mean and variance determined by this observational analysis. The size of each droplet was assumed to be independent of every other droplet, with the same mean value.

Using this method of analysis, the distribution of single jets as they appear during the rotation of the wire electrode could be obtained. An illustrative example is presented in Fig. 7 for the measured current from a wire rotating at 5.6 rpm under an applied

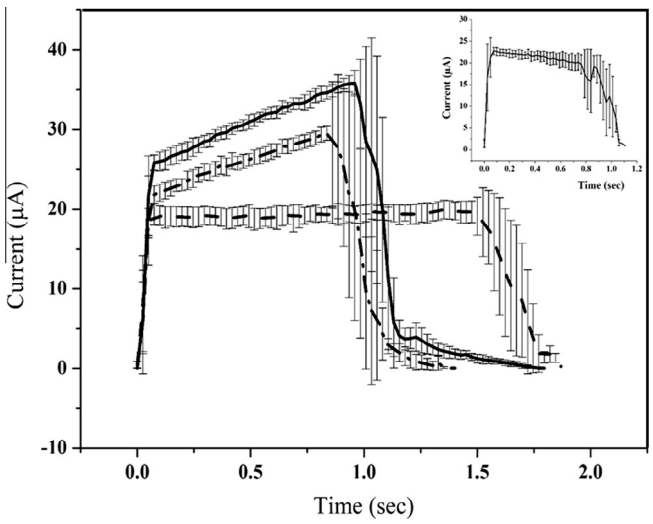

Fig. 6. Average current drawn from a single droplet at 45 kV at rotation rates of 3.2 rpm (dashed), 5.6 rpm (dash dotted), and 8.7 rpm (solid). Error bars correspond to one standard deviation determined from averaging over at least 10 current measurements for single jets. In the inset, the current profile is shown for a single jet that was allowed to jet only after the wire electrode crossed the apex of the arc of rotation (i.e., in between 90° and 203°).

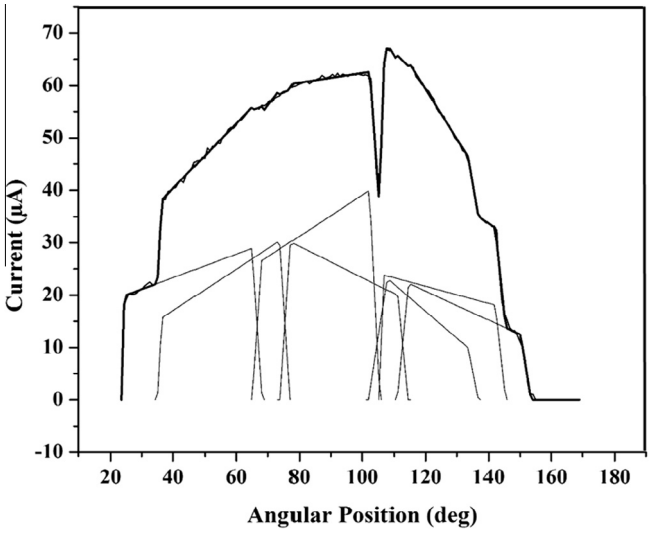

Fig. 7. Optimal model fit to the wire current generated by the Bayesian model, based on piecewise linearity of single jet profiles. The black solid line is the wire current data collected during a free surface electrospinning experiment by rotating the wire spindle at 5.6 rpm with V_{appl} = 45 kV. The heavy solid line that overlaps the data is the best fit obtained from model. The thin solid lines in the figure represent different single jets as they appear at different angular positions in order to generate the total current from the wire.

potential of V_{Appl} = 45 kV. The figure also shows the best fit set of single jets that reproduce the current profile of the wire.

3.6. Linear density of jets

The linear density of droplets jetting concurrently was obtained by dividing the total number of jets at a particular time point by the length of the wire electrode. The linear density of jets as a function of angular position is shown in Fig. 8(a), and is not symmetrical about the apex of the arc of rotation of electrode (i.e., around 90°) as might have been expected. Rather, the linear density of jets is symmetric about an angular position of ~123°. For lower rotation rates, the linear density of jets drops off to zero at a smaller angular position than for higher rotation rates. This suggests that all the droplets formed on the wire at low rotation rates jetted to completion, whereas at high rotation rates jetting was not complete until the wire dived into the bath again, since very few droplets jetted simultaneously. The linear density of jets is one order of magnitude lower than that observed in case of PVA/ethanol.

The linear density of jets is shown as a function of electric field in Fig. 8(b). Shortly after jet initiation at ~38 kV/cm, the linear density of jets increased rapidly, and similarly for the three different rotations rates shown here. Beyond the apex of rotation, however, the linear density of jets decreased in a manner that depended on the rotation rate. The lower rotation rate exhibited a more rapid decline in density of jets than the higher rotation rate. For modeling purposes, the dependence of linear density of jets on electric field was expressed by two second degree polynomials in two different ranges of angular positions:

$$n_l\ [\text{jets/cm}] = \begin{cases} 0.0026E_w^2 - 0.18E_w + 3.21 & \varphi < 123^\circ \\ -0.0002E_w^2 + 0.03E_w - 0.10 & \varphi \geqslant 123^\circ \end{cases} \quad (5)$$

where φ is the angular position of the wire.

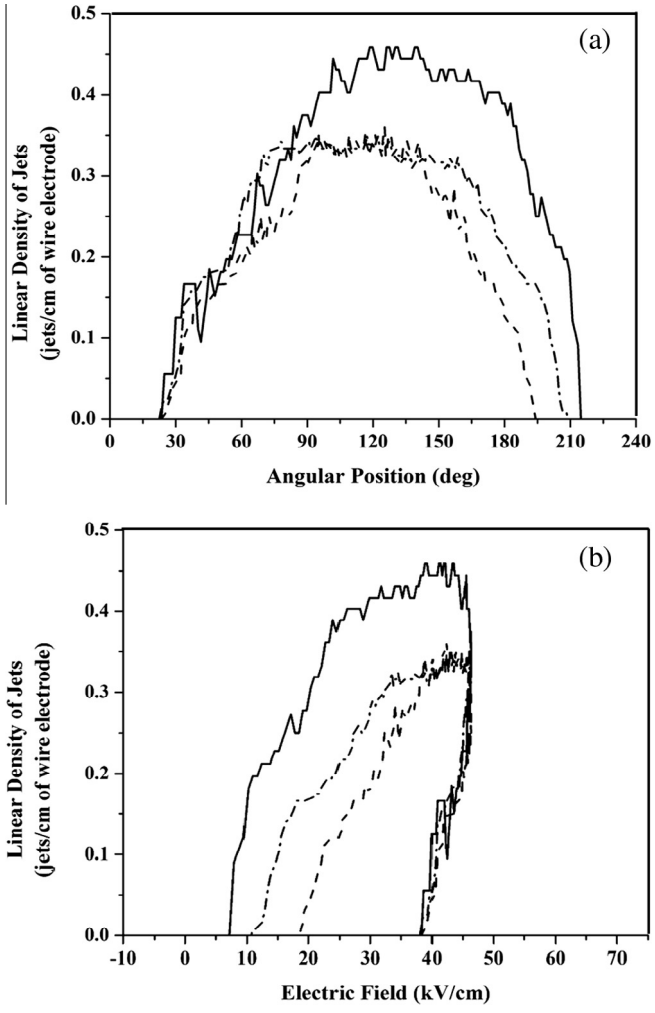

Fig. 8. (a) The linear density of jets as a function of angular position and (b) electric field at different rotation rates: 3.2 rpm (dashed), 5.6 rpm (dash–dotted), and 8.7 rpm (solid line).

3.7. Productivity model

For free surface electrospinning from a wire electrode, productivity is defined as the total mass of product deposited on the collector per unit of time and length of the wire electrode; this is the same convention as employed earlier by Forward and Rutledge. Productivity was determined from the mass of fibers deposited on the collector as a function of rotation rate of the spindle, for four different applied electric potentials: 40 kV, 42.5 kV, 45 kV, and 50 kV. The productivity model that was developed earlier was modified to fit the current experimental data. As was the case for the PVP/ethanol system, two regimes were observed for free surface electrospinning of the PVA/water system. In the entrainment-limited regime, productivity was determined by the amount of liquid entrained on the electrode and can be estimated using

$$P_E = \pi\Omega C r^2[(aCa^b + 1)^2 - 1], \quad (6)$$

where C is the concentration of polymer, in mass per unit volume, assuming that the amount of liquid entrained does not vary with applied voltage [9].

In the field-limited regime, the productivity was determined by the volumetric flow of liquid from the wire electrode to the collector plate, and can be obtained using

$$P_f = V_d\Omega C n_j = \frac{\lambda r^2 C}{2t_j}[(aCa^b + 1)^2 - 1]\int_{\varphi(E_{init})}^{\varphi(E_{term})} n_c(E_w(\varphi'))d\varphi' \quad (7)$$

where n_j is the number of jets emitted from the wire electrode during one single rotation of the spindle; E_{init} is the critical voltage at which jetting is first observed ("initiation"); $\varphi(E_{init})$ is the angle at which such jet initiation is observed for a given applied voltage, as determined by Eq. (2) using $E_w = E_{init}$ = 38 kV/cm; and $\varphi(E_{term})$ is the angle at which jet termination is observed for a given applied voltage and rotation rate. For purposes of this work, the upper limit for jetting was set to be 203°, as observed from experiments. The liquid entrained was considered to be independent of applied voltage and only a function of capillary number. Both experimental and predicted productivities were considered to be valid for one or more wires, as long as the wires were not close enough to influence the electric field of the other.

The productivities measured experimentally at the four different applied voltages are plotted as functions of rotation rate in Fig. 9. Also shown are the productivities predicted by Eqs. (6) and (7) for the entrainment-limited and field-limited regimes, respectively. The model for the field-limited regime, P_F, in particular, shows good agreement with the experimental data. Although the linear density of concurrent jets was only measured at 45 kV, the model predicts the productivity observed at other applied voltages reasonably well.

By applying the model to PVA/water, a significantly different system than PVP/ethanol, the general form of the model and the basic physics behind the model are shown to be robust. Keeping the general form of the model the same as earlier, with only a

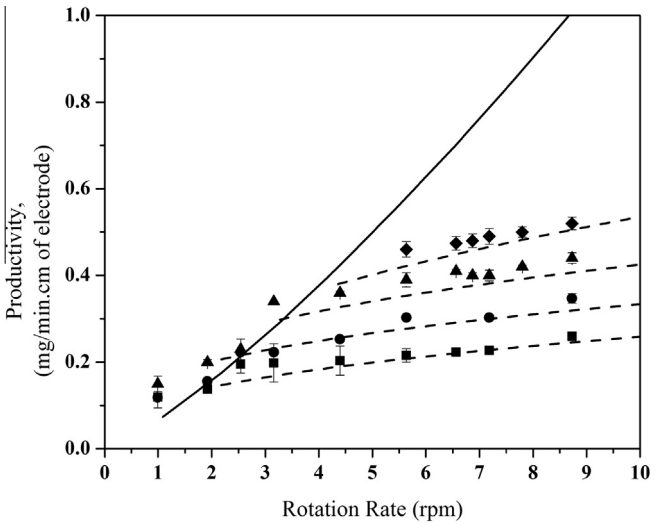

Fig. 9. Model fitting to the experimental productivity data. Experimentally observed productivity (filled symbols) at different rpms at applied potentials of 40 kV (square), 42.5 kV (circle), 45 kV (triangle), and 50 kV (diamond). The entrainment-limited productivity as calculated from Eq. (6) is shown by the solid line and the field-limited productivities at different applied potentials as functions of rotation rate are shown by dashed lines. The transition from the entrainment-limited regime to the field-limited regime is most apparent in the data at 45 kV.

few modifications, the model can predict productivities for two completely different systems. Also, based on the observations for both systems, it remains desirable to operate the free surface electrospinning experiment from the wire electrode at high potentials and at high rotation rates. However, for the PVA/water system, the field-limited regime is reached at a much lower rotation rate than was the case for the PVP/ethanol system, and a higher applied potential is required to initiate jetting. These observations are believed to be due to the higher viscosity and higher surface tension of the aqueous polymer system relative to the ethanol-based system. Also, at a particular desired electric field for electrospinning, the rotation rate at which the transition occurs from entrainment-limited to field-limited regime should be picked for operation with optimal performance.

4. Conclusion

The analytical model that was previously developed for polymeric solution in organic solvent has been applied to an aqueous polymeric solution. This model, with only a few empirically determined parameters, proved to be sufficiently robust to describe two very different types of systems. The relationship for entrainment of the aqueous PVA solutions on the wire was found to be only slightly different from that reported for the PVP/ethanol solutions, which we have attributed to the higher viscosity of the PVA solutions. By contrast, in the present case, the thickness of the entrained liquid layer was comparable to the wire diameter, which is quite different from the earlier observations for PVP/ethanol. Satellite droplets formed, comprising ~3% of the volume of annular film of liquid, but they did not lead to jet formation under the potential applied in these experiments So, although the volumes of these small droplets were considered for purposes of correlating the thickness of the liquid layer with capillary number, they were subtracted when estimating "entrainment-limited" productivity. This treatment proved to be appropriate, as the model could predict the experimental data quite well.

Once again, there exists a critical field for aqueous systems, just like organic systems. For aqueous systems, the magnitude of the critical field was larger; we attribute this to a higher viscosity and higher surface tension of the aqueous solutions.

As seen earlier, two limiting regimes for productivity were observed in the case of aqueous polymeric solution electrospinning. When the rotation rate of the electrode spindle is relatively low, the productivity is limited by the liquid entrainment on the wire. Under this situation, all the liquid entrained on the wire can be converted into jets during the rotation of the electrode as long as the electric field is sufficiently high. In the second regime, when the rotation rate of the electrode spindle is high, there are two limiting factors that come into play in particular for viscous aqueous polymeric solutions. First, the time required for Plateau–Rayleigh breakup of the annular film needs to be sufficiently small such that the highly curved surfaces of the droplets are formed before the wire reaches the critical field. Second, the wire rotation speed needs to be slow enough such that all the droplets have sufficient time to jet before the wire again dives into the solution bath. Thus, this second regime is limited by the angular range of jetting as well as the Plateau–Rayleigh breakup time.

The analysis presented here for aqueous polymeric systems, along with the previous one for ethanol-based polymeric systems, provides a platform to understand the productivity behavior from a free surface electrospinning setup. The key parameters by which the productivity of such a process can be characterized and optimized are not only the applied electric potential, but also the rotation rate of the spindle, spindle geometry (wire diameter, length, number of wires and distance between the wires) and fluid properties.

In closing, we mention that in a recently modified free-surface electrospinning configuration, one or a set of stationary wires is used, with a solution shuttle that coats the solution onto the wire as it moves back and forth along the wires. This configuration eliminates the angular dependence of electric field associated with the rotating spindle, and the several complications arising therefrom. Nevertheless, the model presented here should be applicable as well to this modified configuration, with only minor changes.

Acknowledgement

This work is funded by the MIT-Novartis Center for Continuous Manufacturing.

Appendix A. Supplementary data

Supplementary data associated with this article can be found, in the online version, at http://dx.doi.org/10.1016/j.cej.2015.12.067.

References

[1] S. Ramakrishna, K. Fujihara, W.-E. Teo, T.-C. Lim, Z. Ma, An Introduction to Electrospinning and Nanofibers, World Scientific Publishing Company, 2005.
[2] S. Ramakrishna, K. Fujihara, W.-E. Teo, T. Yong, Z. Ma, R. Ramaseshan, Electrospun nanofibers: solving global issues, Mater. Today 9 (2006) 40–50.
[3] O. Dosunmu, G. Chase, W. Kataphinan, D. Reneker, Electrospinning of polymer nanofibres from multiple jets on a porous tubular surface, Nanotechnology 17 (2006) 1123.
[4] G. Kim, Y.-S. Cho, W.D. Kim, Stability analysis for multi-jets electrospinning process modified with a cylindrical electrode, Eur. Poly. J. 42 (2006) 2031–2038.
[5] S.A. Theron, A.L. Yarin, E. Zussman, E. Kroll, Multiple jets in electrospinning: experiment and modeling, Polymer 46 (2005) 2889–2899.
[6] J. Varabhas, G. Chase, D. Reneker, Electrospun nanofibers from a porous hollow tube, Polymer 49 (2008) 4226–4229.
[7] D. Lukas, A. Sarkar, P. Pokorny, Self-organization of jets in electrospinning from free liquid surface: a generalized approach, J. Appl. Phys. 103 (2008) 084309.
[8] G.G. Chase, J.S. Varabhas, D.H. Reneker, New methods to electrospin nanofibers, J. Eng. Fibers Fabr. 6 (2011) 32–38.
[9] K.M. Forward, G.C. Rutledge, Free surface electrospinning from a wire electrode, Chem. Eng. J. 183 (2012) 492–503.
[10] T.B. Green, S.L. King, L. Li, Apparatus and method for reducing solvent loss for electro-spinning of fine fibers, 2010, U.S. Patent No. 7,815,427.

[11] O. Jirsak, P. Sysel, F. Sanetrnik, J. Hruza, J. Chaloupek, Polyamic acid nanofibers produced by needleless electrospinning, J. Nanomater. 2010 (2010) 49.
[12] E. Kostakova, L. Meszaros, J. Gregr, Composite nanofibers produced by modified needleless electrospinning, Mater. Lett. 63 (2009) 2419–2422.
[13] T. Miloh, B. Spivak, A. Yarin, Needleless electrospinning: electrically driven instability and multiple jetting from the free surface of a spherical liquid layer, J. Appl. Phys. 106 (2009) 114910.
[14] J. Varabhas, S. Tripatanasuwan, G. Chase, D. Reneker, Electrospun jets launched from polymeric bubbles, J. Eng. Fibers Fabr. 4 (2009) 46–50.
[15] X. Yan, J. Marini, R. Mulligan, A. Deleault, U. Sharma, M.P. Brenner, G.C. Rutledge, T. Freyman, Q.P. Pham, Slit-surface electrospinning: a novel process developed for high-throughput fabrication of core-sheath fibers, PloS One 10 (5) (2015).
[16] C. Luo, S.D. Stoyanov, E. Stride, E. Pelan, M. Edirisinghe, Electrospinning versus fibre production methods: from specifics to technological convergence, Chem. Soc. Rev. 41 (2012) 4708–4735.
[17] F.L. Zhou, R.H. Gong, I. Porat, Mass production of nanofibre assemblies by electrostatic spinning, Polym. Int. 58 (2009) 331–342.
[18] X. Wang, H. Niu, X. Wang, T. Lin, Needleless electrospinning of uniform nanofibers using spiral coil spinnerets, J. Nanomater. 2012 (2012) 1–9.
[19] S.L. Goren, The instability of an annular thread of fluid, J. Fluid Mech. 12 (1962) 309–319.
[20] B. Carroll, The accurate measurement of contact angle, phase contact areas, drop volume, and Laplace excess pressure in drop-on-fiber systems, J. Colloid Interface Sci. 57 (1976) 488–495.
[21] S.V. Fridrikh, J.H. Yu, M.P. Brenner, G.C. Rutledge, Controlling the fiber diameter during electrospinning, Phys. Rev. Lett. 90 (2003) 144502.
[22] F. Goucher, H. Ward, The thickness of liquid films formed on solid surfaces under dynamic conditions, Phil. Mag. 44 (1922) 1002–1014.
[23] D. Quéré, Fluid coating on a fiber, Ann. Rev. Fluid Mech. 31 (1999) 347–384.
[24] M.Y. Shin, M.M. Hohman, M.P. Brenner, G.C. Rutledge, Electrospinning: a whipping fluid jet generates submicron polymer fibers, Appl. Phys. Lett. 78 (2001) 1149–1151.